Modelling of $CaBr_2$ Ions Transport Through Ceramic Nanofiltration Membrane

Rasha A. Hajarat*
hajarat@mutah.edu.jo
Hadeel Alfasatleh
Rawan Alhgaish
SalamNader

Abstract

Nernst-Planck equation was used to try to understand the separating behaviour of Ca^{2+}, and Br^- ions using nanofiltration membrane. The model was run for different membrane pores, different volumetric flux based on the membrane area values, and different ions concentration; to study the rejection behavior. In general, as the membrane pore radius increased, the rejection of Ca^{2+} and Br^- ions decreased; where the rejection of Ca^{2+} ion was the higher than the rejection of Br^- ion. While the rejections of Ca^{2+} and Br^- ions increased as volumetric flux based on the membrane area increased. On the other hand, the concentration of Br^- inside the membrane active layer was the higher than the concentration of Ca^{2+} ions. Thus the ions rejection is effected by the membrane pore radius beside the volumetric flux based on the membrane area

Keyword: Nanofiltration, membrane, ion, pore radius, rejection, volumetric flux.

نمذجة نقل أيونات CaBr2 من خلال غشاء الترشيح النانوي الخزفي

* Chemical engineering department, engineering college, Mu’tah University.
Received: 11/4/2021. Accepted: 22/2/2022.

رشا عامر حجرات*

هديل الفساطلة

روان الهقيش

سلام نادر

ملخص

تم استخدام معادلة Nernst-Planck لمحاولة فهم سلوك فصل Ca^{2+} وBr^{1-}. أيونات باستخدام غشاء الترشيح النانوي. تم تشغيل النموذج لمسام غشاء مختلفة، وتدفق حجمي مختلف بناءً على قيم مساحة السطحية للغشاء، وتركيز أيونات مختلفة؛ لدراسة سلوك الفصل الأفضل. بشكل عام، كلما زاد نصف قطر مسام الغشاء، انخفض فصل Ca^{2+} وBr^{1-}. أيونات؛ حيث كان نسبة فصل أيون Ca^{2+} أعلى من نسبة فصل أيونBr^{1-}. بينما زاد نسبة فصل Ca^{2+}و Br^{1-} أيونات مع زيادة التدفق الحجمي بناءً على مساحة الغشاء الطحية. من ناحية أخرى، كان تركيز Br− داخل الطبقة النشطة للغشاء أعلى من تركيز أيونات .Ca^{2+} وبالتالي فإن نسبة فصل الأيونات يتأثر بنصف قطر مسام الغشاء بجانب التدفق الحجمي بناءً على المساحة السطحية للغشاء.

* قسم الهندسة الكيميائية، كلية الهندسة، جامعة مؤتة.

تاريخ تقديم البحث: 2021/4/11. تاريخ قبول البحث: 2022/2/22م .

Introduction:

In biology, Membrane is a very thin layer which forms the out layer boundary of a living cell and the out layer of the internal cell compartments (Bowen & Welfoot, 2002). This layer separates the cell and its compartments from the surroundings, also allows materials to pass into and out of the cell and its compartments. In chemical engineering; the same concept is applied for membrane in separating materials from solutions such as ions, organic material, and bacteria, which is an alternative approach to conventional processes due to its high potentialities (Labbana et al., 2017).

Membrane technology is a separation processes; it's defined as a barrier to certain components while being permeable to others which helps the transport of substances between two fractions. Membrane technology has become a distinguished separation technology over the different separation processes such as flocculation, sediment purification techniques, adsorption (sand filters and active carbon filters, ion exchangers), extraction and distillation (Bodzek, Tomaszewska et al., 2017). Membranes are used in treatment of groundwater, surface water or wastewater. Membrane technology advantages that the membrane works without the addition of chemicals, a relatively low energy consumption, easy, and well-arranged process. The membrane principle is simple: where the membrane acts as a very specific filter that lets water molecule flow through, while it prevents suspended solids and other substances. The efficiency of a membrane filtration process is determined by its selectivity and productivity.

Membrane filtration technology is divided into micro and ultra-filtration and nanofiltration and reverse osmosis (Alsalhya et al., 2018). Micro-filtration and ultra-filtration membranes are used for the removal of large particles. However; when small size contaminants need to be removed from water, then nanofiltration (NF) and/or reverse osmosis (RO) are applied.

This project is about studying the theoretical separation behaviour of $CaBr_2$ salt from brackish water using ceramic Nanofiltration membrane. Ceramic Nanofiltration membrane was chosen; because of their mechanical robustness, chemical and thermal stability, high separation accuracy, and support restrict swelling in comparison with polymer membrane. Nanofiltration membrane is characterised by the Nernst- Planck equation. Nernst-Planck equation describes the solute concentration change inside the

membrane and changes in concentration between feed and permeate streams (Bowen et al., 2002).

Theory:

Transport of ions through Nanofiltration membrane is described by the Extended Nernst-Planck equation; that covers convection and diffusion of ions across nanofiltration membrane. The Extended Nernst-Planck equation includes the following concepts (Bouranene et al., 1 September 2009):

a) Concentration gradient.
b) Electrical potential gradient.
c) Pressure difference across the membrane.

The convection of ions across Nanofiltration membrane is caused by pressure difference across the membrane (Alsalhya et al., 2018). Whereas ion diffusion across Nanofiltration membrane is caused by the concentration and the electrical potential gradients (Labbana et al., 2017). The extended Nernst-Planck equation is presented in equation (1) as follows

$$j_i = K_{i,c} c_i J_v - D_{i,p} \frac{dc_i}{dx} - \frac{z_i c_i D_{i,p}}{RT} F \frac{d\Psi}{dx} \qquad (1)$$

where (j_i) is the flux of ion (i) based on membrane area (mol/m².s), ($D_{i,p}$) is the hindered diffusivity (m²/s), (c_i) is the concentration in the membrane (mol/m³), (z_i) is the valence of ion (i), ($K_{i,c}$) is the hindrance factor for convection inside the membrane, (J_v) is the volume flux based on the membrane area (m/s), (R) is the universal gas constant (8.134 J/mol.K), (T) is the absolute temperature (K), (F) is Faraday constant (C/mol) and (□) is the electrical potential (V). The ion flux is indicated in equation (2) below

$$j_i = C_{i,p} J_v \qquad (2)$$

where ($C_{i,p}$) is the concentration of ion (i) in permeate (mol/m³). The concentration gradient (Bowen et al., 2002) was obtained by substituting equation (2) into equation (1) and rearranging to obtain equation (3)

$$\frac{dc_i}{dx} = \frac{J_v}{D_{i,p}} \left(K_{i,c} c_i - C_{i,p} \right) - \frac{z_i c_i}{RT} F \frac{d\Psi}{dx} \qquad (3)$$

The following assumptions are considered

a) Ideal solution and steady state condition.
b) The membrane effective charge is assumed to be constant, and positive.

c) The electro-neutrality condition in the bulk solution is assumed to be equal to zero (Bouranene et al, 1 September 2009).

1. Integrating and rearranging equation (3), and applying the first two assumptions; subsequently the electrical potential gradient is obtained (Wadekar et al., 2018) as follow

$$\frac{d\Psi}{dx} = \frac{\sum_{i=1}^{n} \frac{z_i J_v}{D_{i,p}} \left(K_{i,c} c_i - C_{i,p}\right)}{\frac{F}{RT} \sum_{i=1}^{n} z_i^2 c_i} \qquad (4)$$

2. The Donnan equilibrium was assumed to apply at the feed/membrane interface and membrane/permeate interface.
3. The Donnan equilibrium is obtained by assuming a diluted solution and the activity coefficient is equal to unity; thus the following equation (5) is obtained:

$$\left(\frac{c_i}{C_i}\right) = \phi \exp\left(-\frac{z_i F}{RT} \Delta\Psi\right) \qquad (5)$$

where $\Delta\Psi_D$ is the Donnan potential (V), C_i is the ion concentration in the solution (mol/m³), and ϕ is the steric partitioning term.

4. Boundary conditions across the membrane active layer are

$$\text{at } x = 0 \longrightarrow C_i = C_{i,f}$$

$$\text{at } x = \Delta x \longrightarrow C_i = C_{i,p}$$

where $C_{i,p}$ is the concentration of ion in the permeate (mol/m³) and $C_{i,f}$ is the concentration of the ion in the feed (mol/m³). Ions rejection (Wadekar & Vidic, 2018) is obtained as follows

$$R = 1 - \frac{C_{i,p}}{C_{i,f}} \qquad (6)$$

The ion concentration inside the membrane was calculated using equation (3), over the assumed boundary conditions (Bouranene et al., 1 September 2009). Then the ion concentration at the permeate side was calculated using equation (5). As a result, the membrane rejection would be calculated by equation (6).

Results and discussion:

Calcium bromide ($CaBr_2$) salt was used; to calculate the rejection of Ca^{2+} and Br^- ions at different physical variables; such as membrane pore radius, and volumetric flux (Hajarat et al., 2020). The module was run over a range of the volume flux based on the membrane active layer surface area (m/s) for a range of membrane pore diameter. The flow rates ranged between 1E-6 to 1E-5 $m^3/m^2/s$, membrane pore radius ranged between 7.0E-10 to 5.0E-9 m, and the initial concentration was assumed to be 1, 5 and 10 mol/m^3. The module was run over a range of the volume flux based on the membrane active layer surface area (m/s) for a range of membrane pore diameter. The membrane thickness was assumed to be equal to 20.0E-6 m, a constant Donnan coefficient equals to 3.89E-3 and held at temperature equals to 298 K.

Calcium ions (Ca^{2+}) rejection:

For calcium bromide salt, the rejections of Ca^{2+} and Br^- increased as the flow rate increased; where the highest rejection was when the flow rate was 1E-5 $m^3/m^2/s$. Besides that, the rejection of Ca^{2+} and Br^- ions increased as the membrane pore diameter decreased. The rejection of Ca^{2+} ions at a flux equal to $1E10^{-5}$ $m^3/m^2/s$ and a membrane pore radius equal to 6E-10 m was around 99%, while the rejection of Br^- was about 96% (figure 1). The rejection of Ca^{2+} ions was higher than the rejection of Br^-, which is due to the assumed membrane charge which was a positive charge. As a result of the membrane positive charge, the rejection of Ca^{2+} ions was higher than Br^- ion, where repulsion occurs between the Ca^{2+} ion positive charge and the membrane positive charge resulting in increasing the rejection of Ca^{2+} ions (Kheriji et al., 2013); where Ca^{2+} ions were retained resulting in high rejection. It was noticed that; as the stokes radius of Ca^{2+} ion to the membrane pore radius ratio increased then the rejection of Ca^{2+} ion increased. The concentration gradient along the membrane active layer for

Ca^{2+} ion was higher than that for Br^- ion (figure 2). As the initial concentration for Ca^{2+} ion increased thenthe concentration gradient along the membrane active layer had a similar trend (Labbana et al., 2017). Where the Ca^{2+} ion concentration decreased from the membrane feed side to the membrane permeate side (figure 2). As the membrane pore radius increased, the rejection of Ca^{2+} ion rejection decreased; thus Ca^{2+} ion passed easily through the membrane because Ca^{2+} ion radius is less that the membrane pore radius (figure 3) (Kheriji et al., 2013).

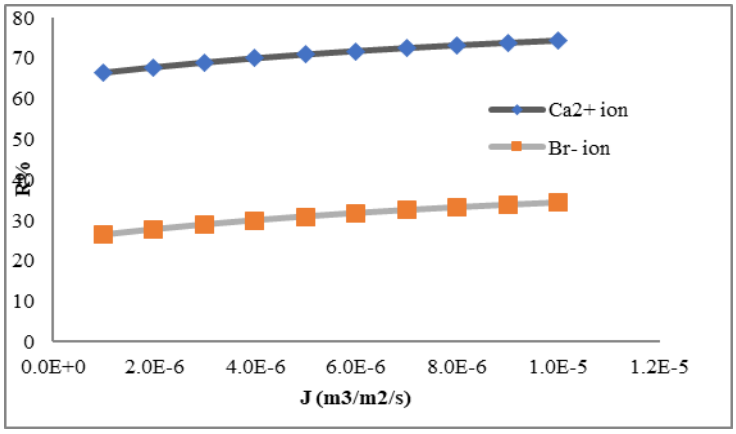

Figure (1) The rejection (R%) for C^{2+} and Br^- ions versus the volumetric flux per membrane surface are (J_v) ($m^3/m^2.s$).

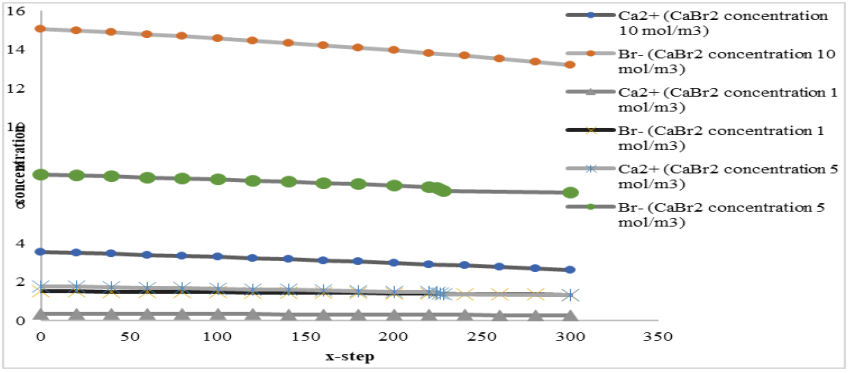

Figure (2) The concentration for Ca^{2+} and Br^- ions versus X-step inside the membrane active layer.

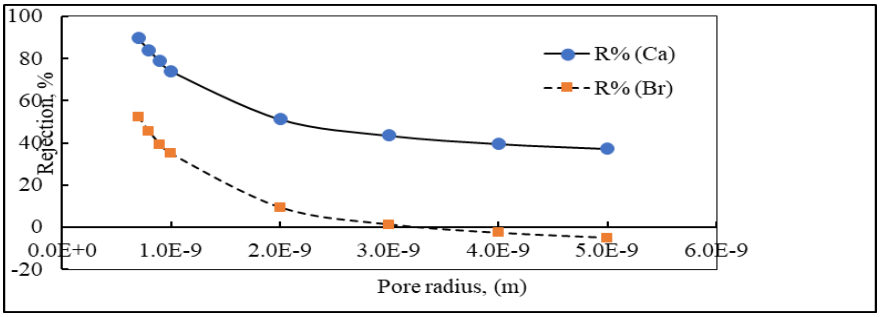

Figure (3) Rejection versus the membrane pore radius

Barium (Br^-) rejection:

As the membrane pore radius increased, the rejection of Br^- ion rejection decreased; accordingly, Br^- ion passed easily through the membrane because Br^- ion radius is less that the membrane pore radius (figure 3). It was noticed that; as the initial concentration for Br^- ion increased then the concentration gradient along the membrane active layer had a similar trend. Where the Br^- ion concentration decreased from the membrane feed side to the membrane permeate side (figure 2) (Nair et al., 2018). The rejection of C^{2+} and Br^- ions increased as the ratio of stokes radius of Ca^{2+} and Br^- to membrane pore radius (□) increased. Other than, the rejection of Ca^{2+} ion was higher than the rejection of Br^- ion, which is supported by the ions radius. Where the Ca^{2+} ion radius is larger than Br^- ion radius, as a result Br^- ion would pass easily through the membrane (figure 4). For both concentration values; 1, 5 and 10 mol/m^3 , it was noticed that the rejection of Ca^{2+} and Br^{1+} ions increased as the volumetric flow rate increased, where the rejection of Ca^{2+} was higher than the rejection of Br^- (Alsalhya et al., 2018).

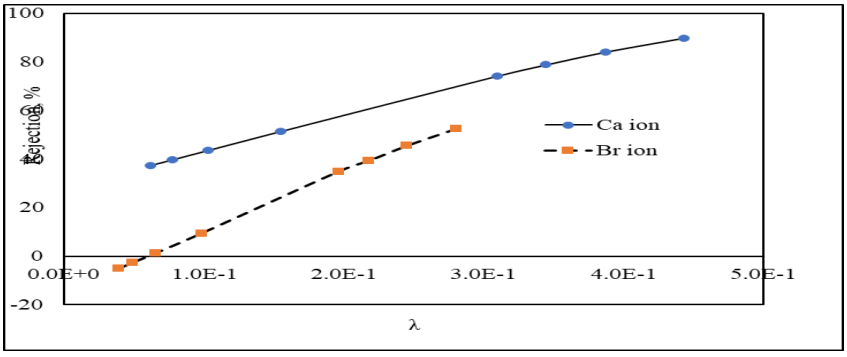

Figure (4) R% versus λ.

Conclusion:

Euler mathematical method was used to solve the extended Nernst-Planck equation; by using FORTRAN programme. The used model to solve the extended Nernst-Planck equation is known for its limitation and for being more descriptive than predictive. The chosen ions were Ca^{2+}, and Br^{-} ions (Wadekar et al., 2018). The model was solved for different feed concentrations, 1, 5 and 10 mol/m^3. The membrane active layer thickness was assumed to be equal to 20.0E-6 m. For each concentration value, the model was solved for different volumetric flux per membrane surface area and membrane pore radius values, where volumetric flux per membrane surface area ranged between 1.0E-6 to 1.0E-5 m^3/m^2.s, and a membrane pore radius values ranged between 7.0E-10 to 5.0E-9 m (Bowen et al., 2002). It was noticed that the ions rejection decreased as the membrane pore radius increased, where the resistance facing the ions decreased which allowed the ions to pass through the membrane. Despite the fact that the membrane pore radius increased where rejection of Ca^{2+} and Br^{-} ions decreased which is a result of the membrane surface charge and the ions charge. The membrane surface charge was assumed be a positive charge, this would assist the rejection behaviour (Kheriji et al., 2013). Where the rejection of Ca^{2+} ion was higher the rejection of Br^{-} ions, where repulsion between of Ca^{2+} ion and the membrane positive effective charge would occur causing the Ca^{2+} ion to accumulate on the membrane surface and be rejected (Nair et al., 2018). On the other hand, the rejection of Br^{-} ion was lower than the rejection of Ca^{2+} ion because the attraction occurring between the Br^{-} ion and the membrane positive effective charge; thus allowing Br^{-} ion to pass easily through the membrane (Wadekar et al., 2018). Thus the membrane positive effective charge and membrane pore radius have an effect on the rejection of ions. More work need to be done in-order to improve this method such understanding the physics of solutions and the properties of ions because they have great effect on the nanofiltration separation process.

Reference:

Alsalhya, Q. F., Mohammed, A. A., Ahmed, S. H., Rashid, K. T., & AlSaadi, M. A. (2018, March). Estimation of nanofiltration membrane transport parameters for cobalt ions removal from aqueous solutions. Desalination and Water Treatment, 108, 235-245.

Ashraf, M. A., Li, X., Wang, J., Guo, S., & Xu, B.-H. (2020, April). DiaNanofiltration-based process for effective separation of Li+ from the high Mg2+/Li+ ratio aqueous solution. Separation and Purification Technology, 247, 116965.

Bodzek, M., Tomaszewska, B., & Rajca, M. (2017). Nanofiltration renovation of mineral water. Archives of Environmental Protection, 43(2), 0-0.

Bouranene, S., Fievet, P., & Szymczyk, A. (1 September 2009). Investigating nanofiltration of multi-ionic solutions using the steric, electric and dielectric exclusion model. Chemical Engineering Science, 64(17), 3789-3798.

Bowen, W. R., & Welfoot, J. S. (2002). Modelling the performance of membrane nanofiltration - critical assessment and model development. Chemical engineering science, 57, 1121-1137.

Hadi, S., Mohammed, A. A., Al-Jubouri, S. M., Abd, M. F., Majdi, H. S., Alsalhy, Q. F., . . . Figoli, A. (2020, June 30). Experimental and Theoretical Analysis of Lead Pb 2+ and Cd 2+ Retention from a Single Salt Using a Hollow Fiber PES Membrane. Membrane, 10(7), 136.

Hajarat, R. A., Hudaib, B., & Al-Awaysah, F. (2020, June). Separating MgBr2, KBr, and NaBr using nanofiltration membrane – Theoretical. International Journal of recent scientific research, 11(6), 38979-38984.

Kheriji, J., Tabassi, D., Bejaoui, I., & Hamrouni, B. (2013). Boron removal from model water by RO and NF membranes characterized using S-K model. Membrane Water Treatment, 7(3), 193-207.

Labbana, O., Liu, C., Chong, T. H., & Lienhard, J. H. (2017, January). Fundamentals of Low-Pressure Nanofiltration: Membrane Characterization,Modeling, and Understanding the Multi-Ionic Interactions in Water Softening. Journal of Membrane, 18-32.

Nair, R. R., Protasova, E., Strand, S., & Bilstad, T. (2018, September 8). Implementation of Spiegler–Kedem and Steric Hindrance Pore Models for Analyzing Nanofiltration Membrane Performance for SmartWater Production. Membranes, 8(3), 78-93.

Wadekar, S. S., & Vidic, R. D. (2018, August 15). Comparison of ceramic and polymeric nanofiltration membranes for treatment of abandoned coal mine drainage. Desalination, 440, 135-145.

Nomenclature:

j_i is the flux of ion (i) based on the membrane area (mol/m².s).

$D_{i,p}$ is the hindered diffusivity (m²/s).

c_i is the concentration in the membrane mol/m³.

z_i is the valence of ion (i).

$K_{i,c}$ is the hindrance factor for convection inside the membrane.

J_v is the volume flux based on the membrane area (m/s).

R is the gas constant (J/mol.K).

r_p is the effective pore radius.

r_i is the radius of component (i).

T is the absolute temperature (K).

F is Faraday constant (C/mol).

Ψ is the Donnan electrical potential (V).

$C_{i,\,p}$ is the concentration of ion (i) in permeate (mol/m³).

$\Delta\Psi_D$ is the Donnan potential (V).

C_i is the ion concentration in the solution (mol/m³).

ϕ is the steric partitioning term.

TMP is transmembrane pressure.

Appendix 1

A. The hindered diffusivity was obtained as follows (Bowen & Welfoot, 2002)

$$\mathbf{D_{i,d} = K_{i,d} D_{i,\infty}} \qquad \text{(a-1)}$$

where $D_{i,\infty}$ is the bulk diffusivity (m^2/s) and $K_{i,d}$ is the hindrance factor for diffusion.

B. The hindrance factor for diffusion is

$$K_{i,d} = K^{-1}(\lambda_{i,0}) \qquad \text{(a-2)}$$

where K is the hydrodynamic drag coefficient.

C. The hindrance factor for convection is

$$K_{i,c} = (2 - \Phi_i) G_{\lambda_{1,0}} \qquad \text{(a-1)}$$

where G is the hydrodynamic drag coefficient and □ is steric partitioning term.

The hydrodynamic drag coefficients (K) and (G) are

$$\mathbf{K^{-1}(\lambda_i, 0) = 1.0 - 2.3\lambda_i + 1.154\lambda_i^2 + 0.224\lambda_i^3} \qquad \text{(a-4)}$$

$$\mathbf{G(\lambda_i, 0) = 1.0 + 0.054\lambda_i - 0.988\lambda_i^2 + 0.441\lambda_i^3} \qquad \text{(a-4)}$$

A. The steric-partitioning term is

$$\boldsymbol{\phi = (1 - \lambda)^2} \qquad \text{(a-5)}$$

where □ is the ratio of ionic or solute radius/pore radius.

B. The stokes radius of component (i) to pore radius ratio (□) is given as follow

$$\boldsymbol{\lambda_i = \frac{r_i}{r_p}} \qquad \text{(a-6)}$$

where r_p is the effective pore radius and r_i is the radius of component (i).

Appendix 2

Sample of the constant parameters that were calculated and used in Fortran programme to run the model.

The hindered diffusivity (Di,p)	
D1,p=Ki,d*Di,∞	D2,p=Ki,d*Di,∞
1.19E-10	7.63E-10
1.80E-10	9.07E-10
2.34E-10	1.02E-09
2.81E-10	1.12E-09
3.21E-10	1.20E-09
5.33E-10	1.58E-09
6.14E-10	1.72E-09
6.57E-10	1.79E-09
6.83E-10	1.83E-09

Figure (5) Hindered diffusivity for Ca^{2+} and Br^{1-} ions.

The hindrance factor for diffusion	
K1,d=K-1	K2,d=K-1
1.51E-01	3.80E-01
2.27E-01	4.51E-01
2.95E-01	5.09E-01
3.54E-01	5.56E-01
4.05E-01	5.95E-01
6.72E-01	7.86E-01
7.75E-01	8.55E-01
8.29E-01	8.90E-01
8.62E-01	9.12E-01

Figure (6) Hindrance factor for Ca^{2+} and Br^{1-} ions.

hindrance factor for convection (Ki,c)	
K1,c=(2-ϕ)(G)	K2,c=(2-ϕ)(G)
1.46E+00	1.43E+00
1.47E+00	1.40E+00
1.46E+00	1.37E+00
1.44E+00	1.35E+00
1.42E+00	1.32E+00
1.27E+00	1.18E+00
1.19E+00	1.13E+00
1.15E+00	1.10E+00
1.12E+00	1.08E+00

Figure (7) Hindrance factor for Ca^{2+} and Br^{1-} ions.

K-1	
ion 1 (Ca)	ion2 (Br)
1.51E-01	3.80E-01
2.27E-01	4.51E-01
2.95E-01	5.09E-01
3.54E-01	5.56E-01
4.05E-01	5.95E-01
6.72E-01	7.86E-01
7.75E-01	8.55E-01
8.29E-01	8.90E-01
8.62E-01	9.12E-01

Figure (8) The hydrodynamic drag coefficient (K) for Ca^{2+} and Br^{1-} ions.